

Nuclide symmetry, stability, and cosmic abundance

Ray Walsh

Professor, Chemistry Dept., College of Western Idaho, USA

raywalsh@cwi.edu

Abstract. The most abundant nuclides in the cosmos have equal numbers of protons and neutrons. These include ^4_2He , $^{12}_6\text{C}$, $^{14}_7\text{N}$, $^{16}_8\text{O}$, $^{20}_{10}\text{Ne}$, $^{24}_{12}\text{Mg}$, $^{28}_{14}\text{Si}$, and $^{32}_{16}\text{S}$, which together comprise 99.5% of ordinary polynucleonic matter. These are the most kinetically resilient (stable) nuclides within the highly exothermic reaction conditions of cosmic nucleosynthesis. This paper analyzes the relationship between a nuclide's equinucleonic ($Z=N$) composition and its relative cosmic abundance. Structural symmetry emerges as a sensitive and specific predictor of superabundance within a proposed alternating nucleon model. The model derives from the proton's radius ($r = 0.8414 \text{ fm}$), the hadron's prolate shape (from the transition to the proton's first excited state, the $\Delta+(1232)$ resonance), and the separation distance between a pair of bound nucleons ($\approx 0.8 \text{ fm}$, from the nucleon-nucleon potential). Various nucleon geometries were considered for each nuclide, with preference given to structures having optimal numbers of stable proton-neutron short-range interactions and whose model radii (derived from the regular polygon radius formula) best correlate with experimental charge radii ($r(31)=.98$, $p<.001$). Remarkably, the best-fit solutions for the eight superabundant $Z=N$ nuclides categorically demonstrate bilateral structural symmetry, in which neutrons reflect protons on opposite sides of a bisecting chiral plane. Conversely, when an element's stable isotopes are compared, the best-fit structures in which nucleon symmetry is *not* possible (generally because proton and neutron numbers are unequal) are less abundant by ≈ 2 orders of magnitude. Symmetry is ubiquitous in nature, and the proposed alternating nucleon model is consistent with the axiom that structural symmetry confers structural stability.

1. Introduction

Protons and neutrons are the smallest units of ordinary matter to have measurable size. The nucleon structure of matter begins with the empirical knowledge of structural and compositional factors leading to the superabundance of light nuclides. These include nuclear shape, sequence and occupancy of nucleons, kinetic stability, and density, addressed here within the framework of a proposed nucleonic cylindrical lattice model. The model's representational coordinate-space geometry is surprisingly straightforward and comprehensible on its own terms.

Introductory textbooks commonly depict protons and neutrons as hard spheres, closely packed within a roughly spherical nucleus. While useful stoichiometrically, empirical evidence suggests that neither nucleons nor nuclei are generally spherical. The charge radii of the larger nuclides may roughly scale with the cube root of the mass number, consistent (in many cases) with a spherical nucleus. [1] However, below ^7Li , the erratic sawtooth radius-to-mass of the lightest nuclides is *not* compatible with sphericity (figure 1). Neither are individual nucleons spherical. The electromagnetic excitation of the nucleon to its first excited state, the Δ resonance, has provided clear evidence of a prolate spheroid

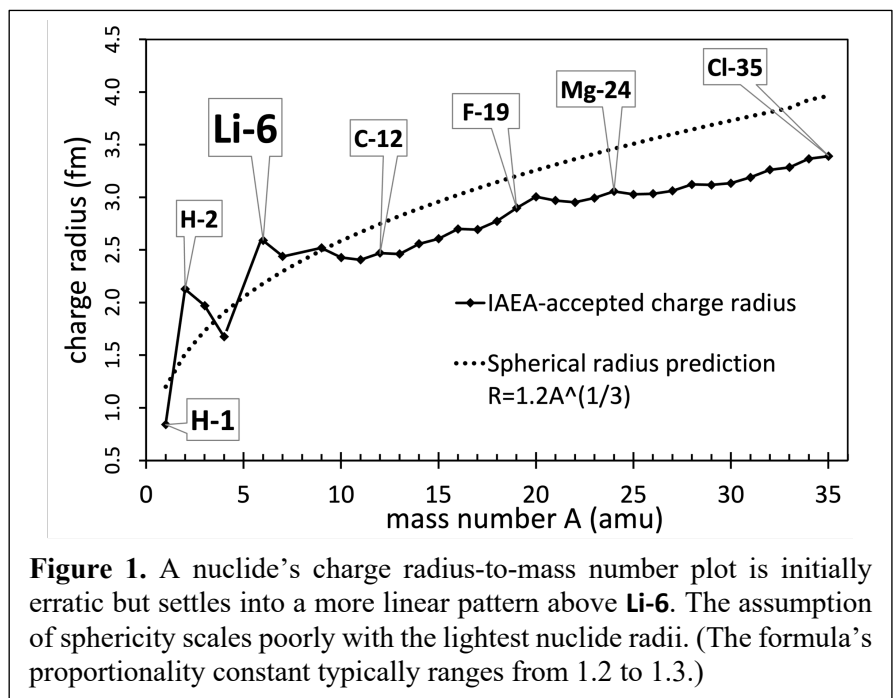


Figure 1. A nuclide's charge radius-to-mass number plot is initially erratic but settles into a more linear pattern above **Li-6**. The assumption of sphericity scales poorly with the lightest nuclide radii. (The formula's proportionality constant typically ranges from 1.2 to 1.3.)

(football shape) deformation of the ground state charge distribution. [2] Atomic spectroscopy of the deuteron (^2H) also indicates a prolate shape. [3] Curiously, the radial charge and point-proton densities of the stable helium isotopes ^3He and ^4He suggest a hole or central depression in the nuclide structure. [4] (^{12}C and ^{16}O demonstrate a similar central dip in their radial charge densities. [5] [6]) And no close-packed nucleon model accounts for the deuteron radius of 2.12 fm, which is oddly larger than the ^4He nucleus of 1.68 fm, even though the latter has twice as many nucleons. [7] This is not consistent with a crystalline lattice of closely packed nucleons, in contrast to the generally constant or flat central charge densities of the medium to heavy nuclides. Given that 99.9% of the ordinary (baryonic) mass of the universe is contained within the lightest nuclides through ^{36}Ar , these curiosities and inconsistencies are no trivial matter.

In addition to nuclide structural factors, nucleon knock-out experiments (in which a projectile impacts a target and the momenta of the fragments are compared) have demonstrated an important compositional factor. Nucleons pair up within nuclei to form short-range correlated pairs (SRCs). [8] (These are predominantly proton-neutron pairs due to the action of the spin-dependent tensor part of the strong nuclear interaction. [9]) More recent knock-out experiments using high-energy *electron* beams directed towards nuclei from carbon to lead demonstrate that *pn* SRC pairs are a universal phenomenon and similar in all nuclei. [10] The *pn* SRC pair represents a prototypic stable proton-neutron *NN* interaction, in contrast to the unstable proton-proton or neutron-neutron interactions. Clearly, the *pn* SRC pair is important and must be accommodated within a comprehensive treatment of the atomic nucleus.

The proton/neutron ratio of the most abundant stable nuclides also bears mentioning. Though hydrogen (the proton) comprises most of the ordinary matter of the universe (74%), when nucleons combine to form the most durable polynucleonic matter, they do so in a one-to-one ratio of protons to neutrons. [11] 99.5% of ordinary baryonic matter by mass (aside from hydrogen) contains equal numbers of protons and neutrons (figure 2). The equality of nucleons is an essential attribute of the kinetically stable forms of matter.

The relationship between nuclide composition and cosmic abundance was a focal point of Maria Goeppert-Mayer's 1963 Nobel lecture: "That nuclei of this type are unusually abundant indicates that the excess stability must have played a part in the process of the creation of elements." [12] She was referring to the *kinetic* stability or durability of nuclides containing "magic numbers" of protons and neutrons (2, 8, 20, 28, etc [13]) created in the highly energetic processes of stellar nucleosynthesis. However, a survey of cosmic abundance indicates that of the top 10 most abundant nuclides [11], only

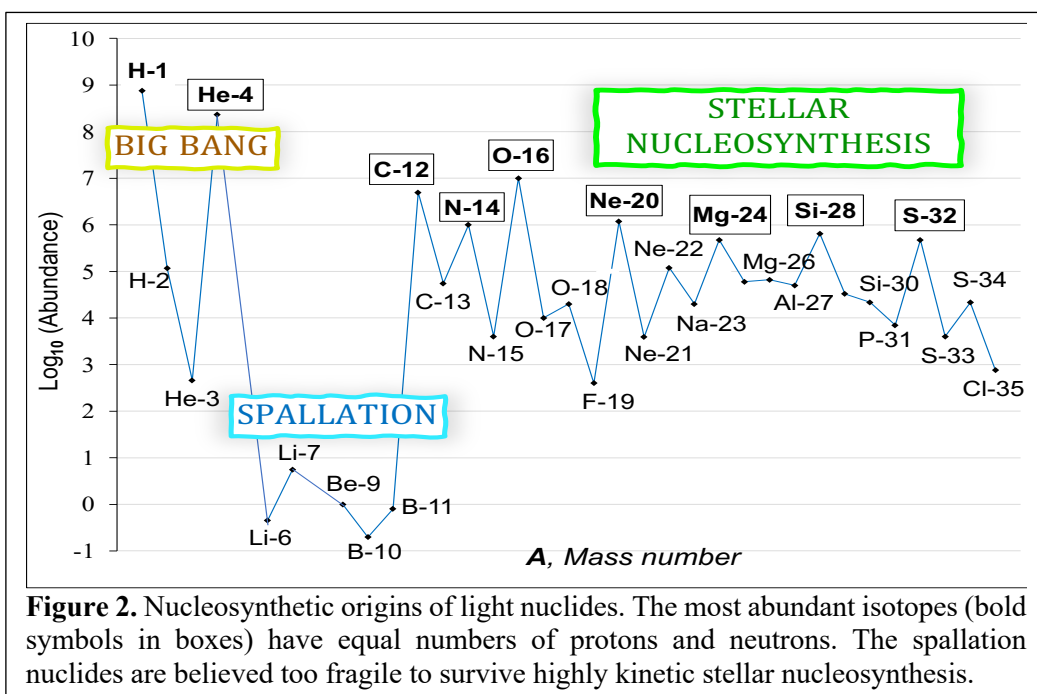


Figure 2. Nucleosynthetic origins of light nuclides. The most abundant isotopes (bold symbols in boxes) have equal numbers of protons and neutrons. The spallation nuclides are believed too fragile to survive highly kinetic stellar nucleosynthesis.

⁴He and ¹⁶O contain magic nucleon numbers. Goeppert-Myers' statement nonetheless speaks to the implicit relationship between a nuclide's kinetic stability and its cosmic abundance. Inasmuch as cosmic abundance implies kinetic stability, the compositional factor that most closely correlates with abundance is the equality of protons and neutrons.

While only two of the ten most abundant light nuclides have magic numbers of protons or neutrons, alpha cluster models demonstrate a higher success rate at anticipating relative cosmic abundance. Seven of the ten most abundant nuclides are alpha nuclides. Exceptions include ¹H, ¹⁴N, and ⁵⁶Fe, whose abundances are predicted by neither the shell model nor alpha cluster models. While the unusually abundant alpha nuclides contain a whole number of multiples of helium nuclei (by definition), the best-fit geometric molecular arrangements of clusters of alpha particles are challenging to reconcile with experimental charge radii. Royer and Eudes report various geometric arrangements of helium nuclei within the nuclides ¹²C, ¹⁶O, ²⁰Ne, ²⁴Mg, and ³²S, yielding respective best-fit radius predictions of 2.43 fm (versus experimental of 2.47 fm), 2.83 fm (vs 2.70 fm), 2.79 fm (vs 3.01 fm), 2.85 fm (vs 3.06 fm), and 3.37 fm (vs 3.26 fm). [14] Although the data set is small, the correlation between predicted and experimental is $r(3)=.87$, $p=.056$, which is not statistically significant at p -value $< .05$. The charge radius predictions of clusters of ⁴He nuclei correlate only loosely with experimental charge radii. This may suggest a rearrangement of nuclear material into nuclide geometries consistent with experimental, perhaps as a final step in the alpha process.

Quantum Monte Carlo (QMC) methods provide the most accurate picture of interactions at the nucleonic level. The approach is not intended for the introductory-level science student, but the generally spectacular results offset the complexity. Many of the basic properties of nuclei can be obtained from mean-field approximations (as opposed to 3D coordinate-space geometric systems), which replace interactions between individual particles with an average effective interaction or "molecular field." [15] Carlson et al. present an overview of nuclear physical properties (including point-proton radii) for $A \leq 12$ nuclear ground states using Green's function Monte Carlo methods (GFMC) in TABLE I of a review article. [16] Computational difficulties limit current GFMC simulations to few-nucleon systems, so the data set is limited, but the point-proton radii r_p of included stable nuclide data through ¹²C demonstrate a strong positive correlation with experimental ($r(6)=.99$, $p<.00001$). All values are in fm, and experimental results follow each GFMC r_p prediction in parenthesis: ²H 1.98(1.96), ³He 1.76(1.76), ⁴He 1.43(1.46), ⁶Li 2.39(2.45), ⁷Li 2.25(2.31), ⁹Be 2.31(2.38), ¹⁰B 2.28(3.31), ¹²C 2.32 (2.33).

In addition to structural and compositional factors, a more subtle but equally perplexing challenge relates to the sequence and occupancy of nucleons within nuclides through ³⁶Ar. The list of stable

nuclides progresses stepwise, one nucleon at a time, except for the unstable 5 and 8 amu nuclides. Why isobars of these two nuclides are unstable and why the sequence of stable nuclides progresses one nucleon at a time is unclear. Further confounding the matter, the selection of either a proton or a neutron during each successive step of the sequence appears random. A complete structural model of the atomic nucleus ought to predict why the addition of one type of nucleon (and not the other) would result in the next stable nuclide while somehow accommodating the disruption in the stepwise sequence at the 5 and 8 amu nuclides.

Again, the compositional factor that most closely correlates with nuclide abundance is an equality of protons and neutrons. This factor is clearly necessary, but apparently not sufficient, for nuclide durability. Both ${}^6\text{Li}$, ${}^8\text{Be}$, ${}^{10}\text{B}$, and ${}^{36}\text{Ar}$ have equal numbers of protons and neutrons but are among the rarest of naturally occurring nuclides. [11] Conversely, ${}^{56}\text{Fe}$ is one of the top 10 most abundant nuclides, having an *unequal* number of nucleons (26 protons versus 30 neutrons). Its unusual abundance may arise out of the formation of ${}^{56}\text{Fe}$ as one of the last exothermic (thermodynamically favored) fusion reactions in the nucleosynthetic chain, resulting in the accumulation of ${}^{56}\text{Fe}$ as an end product of supernovae nucleosynthesis. [17]

While the lighter nuclides are generally more abundant than heavier nuclides (see figure 2), the elements lithium, beryllium, and boron are \approx five orders of magnitude *less* abundant than the next three heavier elements, carbon, nitrogen, and oxygen (from which they derive). [11] All six are initially produced by stellar nucleosynthesis, a highly kinetic environment that subjects nuclei to what structural engineers might term a “dynamic impact load.” [18] However, the fragile isotopes of lithium, beryllium, and boron (along with ${}^3\text{He}$) are thought to be destroyed shortly after formation. [19] Instead, their natural occurrence is a result of spallation, a process involving the fission by a cosmic rays of carbon, nitrogen, and oxygen, respectively. [20]

A clue to the implied structural fragility of the spallation nuclides may arise from the difference in the charge radius determinations obtained from *electron* scattering versus *muon* scattering experiments. [21] In Angeli’s 1999 table of nuclear radii, the seven *e*-scattering radius measurements for ${}^6\text{Li}$ range from 2.38 to 2.76 fm, \approx 25% smaller than those produced by the three μ -scattering determinations ranging from 3.1 to 4.2 fm. From the same table, the 25 *e*-scattering measurements for ${}^{12}\text{C}$ range from 2.35 to 2.53 fm, largely overlapping the ten μ -scattering determinations ranging from 2.40 to 2.60 fm. Additionally, the ${}^{12}\text{C}$ determinations are significantly more precise, regardless of method. Since the muon is \approx 200 times as massive as the electron, the impact of heavier muons may deform and distort the fragile ${}^6\text{Li}$ nucleus while having minimal effect on the durable ${}^{12}\text{C}$ nucleus. Angeli’s updated 2013 table of nuclear radii conveys similar information relating to the errors and uncertainties of radius determination within the term $\Delta_{tot} R$ (fm). The scarcity of the spallation nuclides coincides with the magnitude of their $\Delta_{tot} R$. [7] For relatively fragile (and scarce) ${}^6\text{Li}$, the $\Delta_{tot} R = 0.0390$ fm is more than an order of magnitude larger than the relatively durable (and abundant) ${}^{12}\text{C}$ $\Delta_{tot} R = 0.0022$ fm. This pattern extends generally to all spallation nuclides versus the significantly more abundant equinucleonic nuclides. Presently, no structural model of the atomic nucleus easily accounts for the structural fragility that leads to the scarcity of lithium, beryllium, and boron.

Here, we present a 3D coordinate-space model that is rigorously consistent with the accepted empirical knowledge of the atomic nucleus and yet remains accessible across all disciplines of science. Best-fit structures correlate near-perfectly with IAEA-accepted charge radii for all stable nuclides between ${}^1\text{H}$ and ${}^{36}\text{Ar}$. Structures below ${}^7\text{Li}$ assume various geometries, while above ${}^7\text{Li}$ nuclide structures build upon progressively larger anisotropic cylindrical lattices of alternating protons and neutrons. Remarkably, one end of the anisotropic nuclear cylinder exhibits steric features that determine the sequence and occupancy of successive nucleons, which generally favor the formation of stable proton-neutron NN interactions and pn SRC pairs. Within the parameters of the model, nuclides exhibiting bilateral symmetry predict cosmic abundance, while those isotopes in which symmetry is not possible (generally because proton and neutron numbers are unequal) correlate with scarcity.

2. The Model

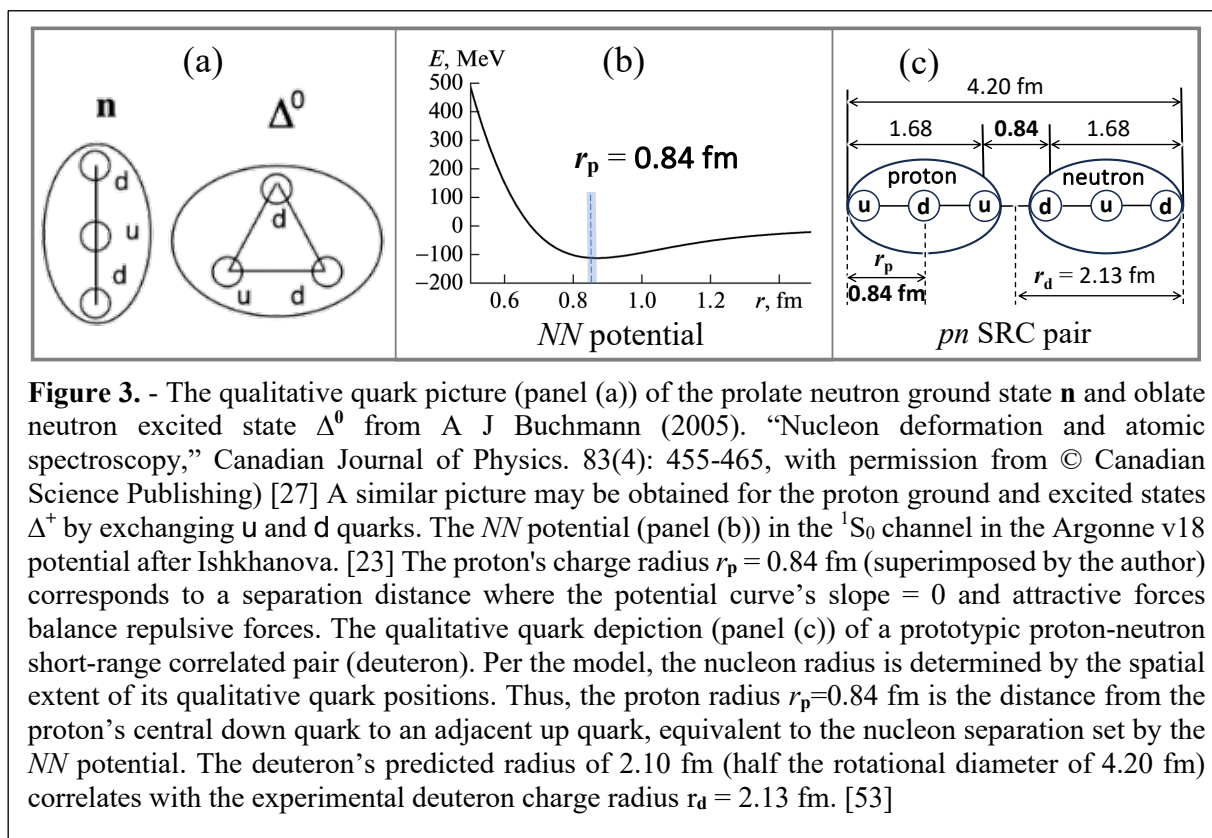
If atomic nuclei are bound systems of discreet protons and neutrons, a geometric representation of the nucleus must include both the size and shape of the nucleon in addition to the separation between them.

The NN interaction determines this separation. It is derived phenomenologically and depends on factors such as spin, alignment, orbital motion, and local nuclear environment. Commonly used NN potentials include the Argonne AV18 potential, as well as the Paris, CD-Bonn, and Nijmegen potentials. [22] The minus derivative of the potential yields the force between a pair of bound nucleons, which is short-range and dependent on the distance between them (figure 3(b)). The interaction is repulsive below $r = 0.7$ fm, but above this threshold, the interaction is attractive, reaching maximal attraction at ≈ 0.8 fm. [23] The result is a potential well that maintains the distance between bound nucleons around a nadir wherein attractive and repulsive forces balance.

The shape of the hadron is also relevant to the coordinate space packing of nucleons. Multiple studies of the intrinsic quadrupole moment of the proton have led to the expectation of a non-spherical nucleon shape. These studies analyze the transition to the first excited state of the nucleon, the $\Delta(1232)$ resonance. [24] [25] [26] [2] figure 3(a) illustrates one perspective on the ground and excited states of the neutron. [27] The proton and neutron have nearly the same mass (938 MeV) and are otherwise identical in every respect except charge. Buchman (2005) suggests that the repulsive spin-spin state between like-flavored quarks and the attractive spin-spin state between unlike-flavored quarks positions the pair of *like* quarks at opposite ends of the prolate nucleon, leaving the *unlike* quark in the center. [27]

The spatial extent of the qualitative linear representation of quark triplets produces the elongated or prolate ground state nucleon shape shown in figure 3(a). This depiction is purely representational as individual quarks have never been isolated, and the uncertainty principle precludes knowing their exact locations and momenta. Additionally, the ground and excited state deformations shown in figure 3(a) appear to result from their respective quark distributions; in reality, each quark is surrounded by a deformed cloud of quarks and antiquarks. [28]

The qualitative quark triplet depiction proves useful in the geometric modeling of nuclide radii regardless of its relationship to reality in a manner perhaps analogous to the depiction of electron pairs in Lewis's dot structures. In the context of the model, qualitative quark depictions imply average quark positions that define the spatial extent of the nucleon. In concert with the separation between nucleons derived from the NN potential (figure 3(b)), the model predicts the deuteron's IAEA-accepted charge

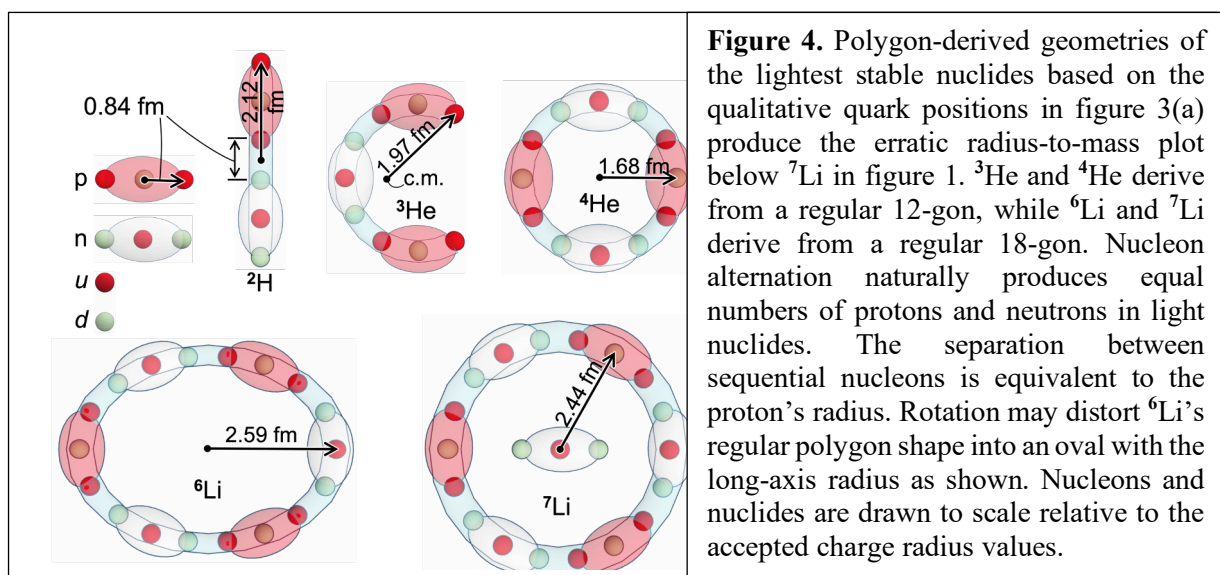


radius remarkably well. The deuteron in figure 3(c) is the prototypic representation of the ubiquitous short-ranged correlated *pn* pair, or *pn* SRC [10], a pair of strongly interacting nucleons whose distance of separation is comparable to their radii. The force is the negative gradient of the potential energy, so attractive and repulsive forces balance (i.e., the force between nucleons equals zero) at the graph's nadir where the slope of the *NN* potential is zero, defined by Ishkhanova at ≈ 0.8 fm. [23] For the purposes of predicting light nuclide radii, the best fit to experimental occurs when the approximation ≈ 0.8 fm is set specifically equal to the proton's charge radius 0.84 fm. [29] A geometric ball-and-stick representation of the deuteron's quark positions then emerges in which the rotational diameter (4.20 fm) equals the sum of the proton and neutron lengths (1.68 fm each, twice the proton's radius) plus the separation distance between them derived from the *NN* potential (0.84 fm), as shown in figures 3(c) and 4. This yields a rotational radius of 2.10 fm (half of 4.20 fm), a $\approx 99\%$ fit to the experimental deuteron charge radius of 2.13 fm. [29]

This representational quark geometry exemplified by the deuteron applies to the remaining nuclide structures. As shown in figure 3(c), the quark-to-quark spacing *between* nucleons is equivalent to the quark-to-quark spacing *within* nucleons, both equal to 0.84 fm. This leads to a generalizable regular 0.84 fm spacing between sequential average quark positions without regard to nucleon positions. This regular spacing becomes an essential constant when incorporated within the radius formula of a regular polygon (formula 1) to predict the charge radius of ${}^4\text{He}$ and larger nuclides, as shown below.

The list of stable nuclides through ${}^{36}\text{Ar}$ progresses stepwise, one nucleon at a time, and proposed structures will (generally) be addressed in a similar stepwise fashion. The next stable nuclide after the deuteron is ${}^3\text{He}$, but the structure of ${}^4\text{He}$ will be addressed first for the sake of expediency. One candidate structure for ${}^4\text{He}$ is a qualitatively linear arrangement of its 12 quarks. The regular spacing of 0.8414 fm between sequential quarks yields a total length of 9.255 fm and a rotational radius half this at 4.628 fm. This is far greater than the experimental charge radius of ${}^4\text{He}$ 1.6755(28) fm [7], and it becomes necessary to consider a denser arrangement of nucleons. A circular arrangement provides the desired symmetry and density. A better correlation with the experimental charge radius of ${}^4\text{He}$ arises from the qualitative positioning of its 12 quarks on the 12 vertices of a dodecagon (12-gon), shown in figure 4. The predicted radius r derives from the general radius formula of a regular polygon as shown in Formula (1), where a is the distance between two neighboring quarks (0.8414 fm), and the number of sides (or vertices) n equals 12, the number of quarks:

$$r = \frac{a}{2} \csc \left[\frac{\pi}{n} \right] \quad (1)$$



The regular polygon formula predicts a ${}^4\text{He}$ radius of 1.625 fm, which falls within the range values included in Angeli(1999) (1.61-1.70, n=11(*e*-scattering)) [21], and is a close approximation to the IAEA-accepted charge radius of 1.6755(28) fm. [7] Importantly, this point-symmetrical circular isomer is consistent with the empirical knowledge of helium structure, which indicates a hole or central depression in the electron scattering radial charge densities of ${}^3\text{He}$ and ${}^4\text{He}$, as reported by McCarthy et al. [4]

The best-fit structure of ${}^3\text{He}$ derives from the same regular dodecagon structure. ${}^3\text{He}$ has only nine quarks, however, so three of the 12 dodecagon vertices are unfilled. The resulting irregular horseshoe shape (figure 4) shifts the center of mass away from the dodecagon center, precluding the use of the regular polygon formula. The new center of mass must be calculated by weighted average. The predicted radius of rotation is 1.92 fm (versus the accepted charge radius of 1.9661(30) fm [7]), as determined by the distance from the calculated center of mass to the farthest quark (figure 4). The predicted radius of 1.92 fm is well within the range of the ${}^3\text{He}$ charge radius values included in Angeli (1999) (1.84-1.97 fm, n=9 (*e*-scattering)). [21] The shift away from the dodecagon center consequently imparts to ${}^3\text{He}$ a predicted radius larger than ${}^4\text{He}$ (\approx 1.68 fm). Like the circular structure of ${}^4\text{He}$, the resulting horseshoe shape of ${}^3\text{He}$ also has a central depression or a hole in the charge radius, as reported by McCarthy et al. [4] (Many of the remaining light nuclides though ${}^{36}\text{Ar}$ demonstrate a similar central depression in the charge densities. [6])

There is a precipitous drop in abundance after the helium isotopes in the plot of cosmic abundance as there is no stable five amu nuclide. The half-lives of the isobars ${}^5\text{He}$ and ${}^5\text{Li}$ are measured in yoctoseconds (one preceded by a decimal point and 22 zeros), and this mass gap effectively halts the proton-proton nucleosynthetic chain from continuing beyond ${}^4\text{He}$. [30] The alternating nucleon model predicts this mass gap as no five amu nuclide can form an uninterrupted ring of alternating nucleons analogous to the ringed arrangement of nucleons in ${}^4\text{He}$. The proton/neutron bound state is the only stable NN bound state, and at some point, in a closed circular arrangement of five nucleons, there would be an unstable proton-proton or neutron-neutron interaction precluding ring closure.

The radius prediction of ${}^6\text{Li}$ derives from Formula 1 and a qualitative distribution of its 18 quarks into a regular octadecagon (18-gon). The predicted radius of 2.432 fm is within the range of reported charge radius values included in Angeli(1999) (2.38-2.76 fm, n=7 (*e*-scattering)). [21] If the ring arrangement of *four* nucleons in ${}^4\text{He}$ produces a kinetically stable structure (as indicated by its abundance and low $\Delta_{tot}R = 0.0028$ fm [7]), then a ring arrangement of six nucleons may result in a more lax structure for ${}^6\text{Li}$. Ring laxity and nuclear rotation may then distort the octadecagon into an oval (figure 4) with a long-axis radius of rotation closer to the IAEA accepted charge radius of 2.5890(390) fm. [7] Alternatively, as with any lax ring, the structure may demonstrate stable node/anti-node oscillation states [31], in which the long axis of the oval oscillates between 0° and \approx 90°. Furthermore, the proposed non-rigid structure of ${}^6\text{Li}$ may account for its unusually large uncertainty of charge radius measurement ($\Delta_{tot}R = 0.0390$ fm [7]) across an unusually wide range of reported experimental radius values (2.38-2.76 fm) by electron (*e*)-scattering. [21] The significantly larger charge radius values obtained by muon (μ)-scattering (3.1-4.2 fm [21]) may relate to the greater mass of the muon (200x greater than the electron), which may mechanically perturb or distort the ${}^6\text{Li}$ structure during μ -scattering experiments, resulting in a larger muon charge radius.

Subsequent best-fit alternating nucleon structures build upon the ${}^6\text{Li}$ ring by the incremental addition of nucleons, resulting in the more linear radius-to-mass above ${}^6\text{Li}$ shown in figure 1. ${}^7\text{Li}$ is a ${}^6\text{Li}$ ring with a neutron inclusion in the ring's center (figure 4). The neutron inclusion is similar in principle to the orbiting nucleons of a halo nucleus, which mechanically enlarge the experimental charge radius. [32] However, rather than orbiting around the nucleus in a halo, the ${}^7\text{Li}$ neutron inclusion occupies the interior of the nucleus. The included neutron effectively inflates the loose oval of ${}^6\text{Li}$ (with its large long axis radius) into a more rigid ring having an effectively smaller rotational radius. The radius prediction of ${}^7\text{Li}$ is thus the radius of the surrounding six nucleon ring. As with ${}^6\text{Li}$ above, the radius of 2.432 fm is predicted by formula 1 and a regular octadecagonal arrangement of 18 quarks, resulting in a close match to the value accepted by the IAEA 2.4440(0.0420) fm [7], and well within the range of the ${}^7\text{Li}$ charge radius values included in Angeli (1999) (2.38-2.44 fm, n=4 (*e*-scattering)). [21] ${}^7\text{Li}$ is an order of magnitude *more* abundant than ${}^6\text{Li}$, which is atypical. Isotopes having an odd mass

number are generally at least an order of magnitude *less* abundant than the even mass number isotopes to either side. The greater abundance of ^7Li may imply greater kinetic stability. Perhaps the ^7Li neutron inclusion serves as an architectural cross-member that stabilizes the lax ^6Li ring by distributing dynamic impact loads, similar in principle to the function of a cross-member within a bridge truss. [33]

^8Be is an alpha nuclide with a half-life $\approx 10^{-16}$ seconds. The ^8Be mass and instability suggest a transient bound state of two helium nuclei. The present representational model predicts a nucleon sequence in which a proton added to the ^7Li neutron inclusion would create a stable pn SRC pair, and that the SRC would then associate with the ^6Li ring within a $^6\text{Li} + ^2\text{H}$ bound state. The proposed structure is shown in Table 1 below. However, given that there is no stable 8 amu isobar, it may be that the proposed node/anti-node vibrational instability of the lax ^6Li ring structure (as discussed above) might be sufficiently destabilizing to preclude binding to ^2H .

The best-fit alternating nucleon structure of ^9Be combines a ^6Li base ring bound to a 3 nucleon npn sequence on a second incomplete ring, as shown in Table. Using the ring separation value $r_s = 0.9616$ fm determined from the structure of ^{12}C (discussed below), the predicted radius of 2.47 fm is well within the range of the ^9Be charge radius values included in Angeli (1999) (2.20-2.53 fm, n=9 (*e*-scattering)) [21], and a close match to the value accepted by the IAEA 2.5190(0.0120) fm. [7] Importantly, each of the three nucleons on the second ring is associated with its opposite isospin nucleon on the ^6Li base ring to form proton-neutron pairing of another type.

The next two stable nuclides, ^{10}B and ^{11}B , have roughly the same experimental charge radius as ^7Li . All three radii ≈ 2.42 fm, essentially the same radius (2.43 fm) predicted for a regular octadecagon by formula (1) where $n = 18$ quarks (^6Li) and a is the proton's radius (0.8414 fm). Within the model, ^7Li , ^{10}B , and ^{11}B all have a base ^6Li ring structure with the mass of their additional nucleons contained within the interior of the ^6Li ring. Thus, the predicted radii of all three nuclides equate to the radius of the exterior base ^6Li ring. ^7Li has a neutron inclusion, as discussed above, but within the proposed ^{10}B structure, the exterior ^6Li ring loosely includes a ringed four-nucleon ^4He nucleus instead of a neutron. The extremely low cosmic abundance of ^{10}B (see figure 2) is consistent with a loose association between the rings. The proposed structure of ^{11}B is the same as ^{10}B but with an additional neutron tethering the base ^6Li ring to the included ^4He ring. ^{11}B is four times more abundant than ^{10}B , indicating that the added neutron has a stabilizing effect similar to the example of ^7Li . Here we suggest that the added neutron may tether the two rings together, as shown in Table 1. These two nuclides ^7Li and ^{11}B , along with ^{19}F and ^{31}P below, are examples where an additional neutron may structurally reinforce and thus bestow greater durability and abundance. Regardless, the somewhat precarious nature of the proposed spallation nuclide structures is intentional and designed to reflect a measure of expected fragility commensurate with their low relative cosmic abundances.

In mechanical systems, the lamination of flexible materials confers both stiffness and strength. [34] The proposed structure of ^{12}C comprises two stacked ^6Li rings (figure 5) sharing a common geometric axis. The open ring structure is consistent with the central dip in the point-proton density of ^{12}C , as illustrated by Carlson (2015). [16] Although the individual ^6Li rings are lax and fragile within the model, the “lamination” of two ^6Li rings predicts a more rigid and durable structure for ^{12}C , as suggested by its unusually high cosmic abundance and low uncertainty in measurement $\Delta_{\text{tot}} R = 0.0022$ fm. [35] Each ^6Li ring qualitatively distributes 18 quarks on the vertices of a regular octadecagon having sides $a = 0.8414$ fm and $r = 2.432$ fm per Formula 1. The proposed structure of ^{12}C exhibits perfect point symmetry. This implies that the distance from the ^{12}C center of mass to any of its 36 qualitative quark positions is the same and equal to the IAEA-accepted charge radius of 2.4702 fm. The ^{12}C abundance, symmetry, and small uncertainty in measurement ($\Delta_{\text{tot}} R = 0.0022$ fm [35]) are consistent with stability and rigidity, making ^{12}C ideal for setting the standard distance between adjacent parallel rings necessary for predicting the radii of multi-ring structures. The charge radius and perfect point symmetry geometrically fix the ring separation r_s at 0.9616 fm. Additionally, the prolate nucleon has a long-axis radius equivalent to the proton's radius of 0.8414 fm. The 0.9616 fm distance between rings limits the short-axis radius of the prolate spheroid nucleon to half this, or 0.4808 fm, when the nucleon is associated in parallel with an opposite isospin nucleon on an adjacent ring.

^{12}C and ^{13}C have nearly identical radii (2.47 fm and 2.46 fm, respectively), even though ^{13}C has an additional neutron (figure 5). This is similar to the cases of ^7Li , ^{10}B , and ^{11}B discussed above, all three

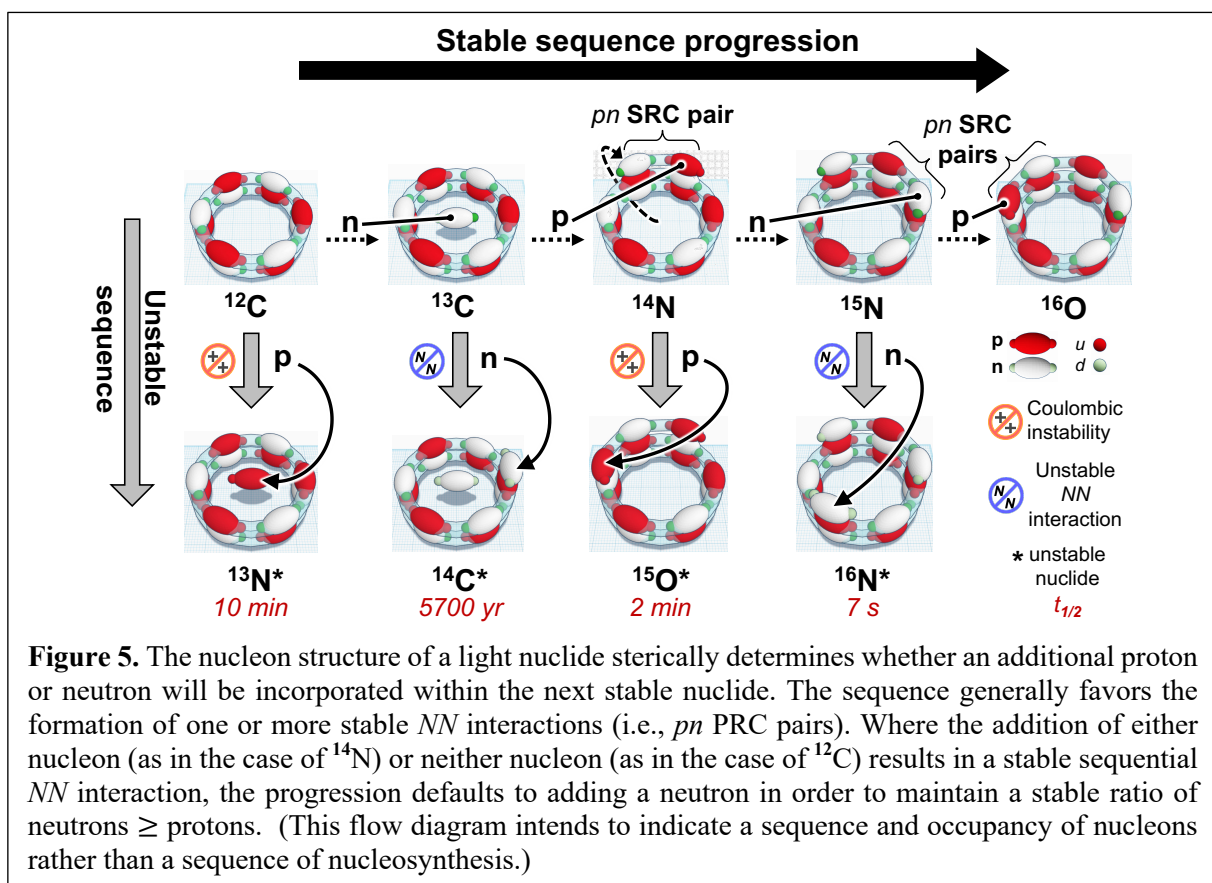


Figure 5. The nucleon structure of a light nuclide sterically determines whether an additional proton or neutron will be incorporated within the next stable nuclide. The sequence generally favors the formation of one or more stable NN interactions (i.e., pn PRC pairs). Where the addition of either nucleon (as in the case of ^{14}N) or neither nucleon (as in the case of ^{12}C) results in a stable sequential NN interaction, the progression defaults to adding a neutron in order to maintain a stable ratio of neutrons \geq protons. (This flow diagram intends to indicate a sequence and occupancy of nucleons rather than a sequence of nucleosynthesis.)

of which have the same charge radius and additional mass contained within a base ^6Li ring. Here, the additional neutron of ^{13}C is included within the ^{12}C structure and, therefore, has a charge radius essentially identical to ^{12}C . The relative abundance of ^{13}C (two orders of magnitude less than ^{12}C) suggests that the additional neutron may not confer structural durability, unlike the neutron inclusions of ^7Li and ^{11}B .

While a *neutron* added to ^{12}C results in a stable product, a *proton* added to ^{12}C may be disfavored for coulombic reasons, given the positive charge on both the ^{12}C nucleus and the proton, and given that unstable ^{13}N (figure 5) would be left with an unfavorable ratio of protons $>$ neutrons. The addition of a proton to ^{13}C , however, results in greater stability as this additional proton links to the central neutron to form a *pn* SRC pair. After calculating the center of mass (COM) and the distance from the COM to the farthest qualitative quark position, the best fit to the experimental radius of ^{14}N places the SRC on a third parallel partial ring (figure 5). The model radius prediction of 2.61 fm is a close match to the value accepted by the IAEA 2.5582(0.0070) fm. [7] An additional neutron to ^{13}C results in an unstable neutron-neutron interaction to form unstable, radioactive ^{14}C (figure 5). (The addition of individual nucleons is *not* intended to indicate nucleosynthetic reactions but rather to indicate a steric role for the sequence and occupancy of nucleons.)

As the sequence progresses, the addition of a neutron to the third parallel partial ring of ^{14}N creates a second *pn* PRC pair with the proton already there, yielding ^{15}N whose predicted radius of 2.61 fm matches the value accepted by the IAEA of 2.6058 (0.0080) fm. Importantly, the addition of a proton to ^{14}N would *also* create a *pn* PRC pair, but forms unstable ^{15}O (figure 5). In this case, the addition of the proton is disfavored for coulombic reasons due to an unfavorable ratio of protons $>$ neutrons.

The model structure of ^{15}N has a three-nucleon *npn* sequence on a third incomplete ring bound to a ^{12}C . The addition of a proton to either of the two neutrons already present on the third ring enhances overall stability by creating a *pn* PRC pair to form stable ^{16}O , with a predicted radius of 2.61 fm as compared to an experimental radius of 2.6991(0.0052) fm. [7] Conversely, there is no placement of an additional *neutron* that would create a *pn* PRC pair. *The steric structure of ^{15}N thus selects which type*

of nucleon may be added to form the next stable nuclide. Figure 5 illustrates a steric selection role in predicting nuclide stability.

The model structure of ^{16}O contains a complete ^{12}C double ring plus a third partially-filled ring containing a sequence of four alternating nucleons beginning with a neutron and ending with a proton (figure 5, upper right). The addition of either a proton to one end or a neutron to the other could create a stable *pn* PRC pair. However, an additional proton would result in an unstable ratio of protons > neutrons, so the addition of a neutron is favored. The next stable nuclide is thus ^{17}O with a predicted radius of 2.73 fm, compared to an experimental value of 2.6932(0.0075) fm. [7]

The structure of ^{17}O contains a ^{12}C double ring and a sequence of five alternating nucleons. The sequence begins and ends with a neutron. Per the aforementioned selection rules, the addition of a proton would bind to both these neutrons, close the ring, and create two new *pn* PRC pairs. The resulting structure is unstable, however. The predicted structure of ^{18}F has a ^6Li ring stacked on a ^{12}C ring. We propose that the instability of ^{18}F relates to the node/antidote vibration of ^6Li (see above), precluding an effective interaction with ^{12}C . The next stable nuclide in the sequence is ^{18}O , whose structure is identical to ^{17}O but with an additional neutron inside the nuclear cylinder. The predicted radius of ^{18}O is 2.74 fm, while the IAEA-accepted radius is 2.7726(0.0056) fm.

Predicted versus experimental charge radii of subsequently described nuclides are featured in Table 1. The intent is to describe the sequence and occupancy of nucleons and not to describe nucleosynthetic processes.

The addition of a proton to ^{18}O results in two additional *pn* SRCs within the next stable nuclide, which is ^{19}F . The model predicts a ^6Li ring stacked on a ^{12}C ring. The structure is similar to ^{18}F , but the node/antidote vibration of ^6Li may be stabilized by the additional neutron in a manner analogous to the role of the tethering neutron in ^{11}B . The addition of a proton to this tethering neutron results in ^{20}Ne , comprising a *pn* SRC pair atop a triplet of ^6Li rings. The addition of either a proton or a neutron to ^{20}Ne could create a stable *pn* PRC pair. However, an additional proton would result in an unstable ratio of protons > neutrons, so the addition of a neutron is favored to produce ^{21}Ne . The model then predicts that only the addition of a proton has the potential to form a *pn* SRC pair, but the resulting ^{22}Na is unstable for reasons not anticipated by the model. Thus, a neutron is added to form ^{22}Ne . The additional model is not able to form a stable *NN* interaction with the *npn* sequence of ^{21}Ne but may be included in the center. The addition of a proton forms two stable *pn* PRCs on an incomplete 4th ring to form ^{23}Na , as shown in Table 1. An additional neutron completes the 4th ring to form ^{24}Mg . An added neutron is included in the cylinder space to form ^{25}Mg . As with ^{21}Ne , the model anticipates the addition of a proton, but this would form unstable ^{26}Al . Instead, a second neutron is included within ^{26}Mg . The addition of a proton results in two additional *pn* PRCs for ^{27}Al within a three-nucleon *npn* sequence on a 5th incomplete ring. An additional neutron to either end of the *npn* sequence would result in a *pn* SRC to form ^{28}Si . The subsequent addition of either a proton or a neutron to the other could create a stable *pn* PRC pair, but the neutron is favored (resulting in ^{29}Si) because an additional proton would create an unstable ratio of protons > neutrons. The model then predicts the addition of a proton to ^{29}Si , but ^{30}P is unstable for reasons perhaps similar to the instability of ^{18}F . The next stable nuclide thus adds a neutron to form ^{30}Si . An additional proton forms two additional *pn* SRCs and completes the 5th ring of ^{31}P , followed by the addition of another proton to form ^{32}S , resulting in another *pn* SRC pair. The subsequent addition of either a proton or a neutron to ^{32}S could create a stable *pn* PRC pair, but an additional proton would result in an unstable ratio of protons > neutrons. Thus, an additional neutron is favored to produce ^{33}S . Similar to the previous, the model then predicts that only the addition of a proton has the potential to form a *pn* SRC pair, but the resulting ^{34}Cl is unstable for reasons not anticipated by the model. Thus, a neutron is added to form ^{34}S . An additional proton results in an additional *pn* SRC pair within ^{35}Cl , followed by the addition of a proton, which completes the 6th ring and forms two additional *pn* SRCs within ^{36}Ar .

2.1. Rotational considerations in radius prediction.

Any rotation in a three-dimensional space can be analyzed using a combination of the three principal axes. [36] Where a rigid body has an axis of symmetry, this axis will correspond to a principal axis of

rotation. The most stable rotational axis is where the greatest mass is distributed the farthest from the rotational axis, and rotation about this major inertia axis corresponds to the minimal kinetic energy.

The model assumes that a nucleus rotates in space and that the manner of rotation determines its spatial extent and, therefore, its radius. The radii of most light nuclides are best predicted by end-over-end tumbling rotation (indicated by italics and preceded by r_T in Table 1), in which case the radius is determined by the distance from its center of mass to its farthest average quark position. This implies a radius of rotation through the nucleus center of mass and orthogonal to the length of the model nuclear cylinder. In some of the lightest nuclides, rotation may look more like the wobble of a plate spinning on a table just before it comes to rest. This type of rotation is called precession, and the method of radius determination assumes the rotational radius is half the distance between the two average quark positions farthest from one another within the proposed nuclide structure. The rotational axis, in this case, passes through the geometric center of the base ^6Li ring and is orthogonal to the geometric plane occupied by the ^6Li ring. For many of the nuclides ^7Li through ^{16}O , the manner of rotation didn't make a difference to the radius prediction. However, in the cases of ^{14}N , ^{15}N , and ^{16}O , the precessing radius (r_P) determinations of 2.61, 2.61, and 2.61 fm (respectively) were a better fit to experimental than the tumbling radius predictions of 2.79, 2.84, and 2.80 fm (respectively). The experimental charge radius of ^{16}O (2.70 fm) is halfway between the precessing prediction of 2.61 fm and the tumbling prediction of 2.80 fm and may represent a mix of the two rotational states. As an aside, the manner of rotation may be a factor in a nuclide's nuclear magnetic moment.

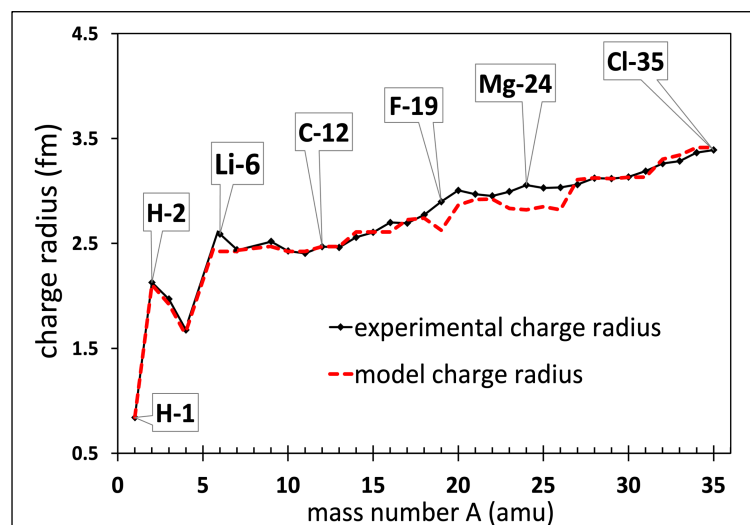


Figure 6. Model charge radius predictions demonstrate strong positive correlation with IAEA-accepted charge radii (black solid line), ($r(31)=.98$, $p<.001$).

3. Results

As shown in figure 6, predicted radii of the proposed structures of the stable nuclides through ^{35}Cl correlate well with experimental except for gaps around ^6Li , ^{19}F , and ^{24}Mg . The radii of these structures derive from the formula of a regular polygon, the proton's radius, the hadron's shape, and proton-neutron separation as determined by the NN potential. The sequence and occupancy of nucleons within proposed structures was predicated on the stability of the pn SRC pair and a stable ratio of neutrons \geq protons.

Within Table 1, each nuclide is enclosed in a box, and below each nuclide symbol is the cosmic abundance cited as the number of atoms relative to silicon, set arbitrarily at one million (1×10^6). The isotopic percentage within an element is shown in parenthesis below this, and for elements that have only one stable isotope, such as ^{23}Na , the number is 100%. Below the graphic depiction of each cylindrical nuclide is the IAEA-accepted charge radius in bold, followed by the model-predicted radius in italics. The assumption here is that nuclei are rotating in space, and the manner of rotation can be

Table 1. Alternating nucleon structures of stable light nuclides through ^{36}Ar

I	II	III	IV	V	VI	VII	VIII	IX	X	XI	XII	
PERIOD ONE	7Li 6×10^0 (92.4%) 2.44 fm $r_T = 2.42 \text{ fm}$ 7.2 MeV +3.26	8Be Unstable $t_{1/2} = 8 \times 10^{-17} \text{ s}$ 2.52 fm $r_P = 2.47 \text{ fm}$ 17.3 MeV -1.18	9Be 1×10^0 (100%) 2.52 fm $r_T = 2.42 \text{ fm}$ 1.6 MeV -1.18	10B* 2×10^{-1} (19.9%) 2.43 fm $r_{T,P} = 2.42 \text{ fm}$ 6.6 MeV +1.80	11B 8×10^{-1} (80.1%) 2.41 fm $r_{T,P} = 2.42 \text{ fm}$ 11.5 MeV +2.69	12C* 5×10^0 (98.9%) 2.47 fm $r_{T,P} = 2.47 \text{ fm}$ 5.0 MeV 0	13C 1×10^4 (1.1%) 2.46 fm $r_{T,P} = 2.47 \text{ fm}$ 7.5 MeV +0.702	14N* 1×10^6 (99.6%) 2.56 fm $r_P = 2.61 \text{ fm}$ 10.9 MeV -0.283	15N 4×10^3 (0.4%) 2.61 fm $r_P = 2.61 \text{ fm}$ 12.1 MeV 0	16O* 1×10^7 (99.8%) 2.70 fm $r_P = 2.61 \text{ fm}$ 4.1 MeV -1.89	17O 1×10^3 (0.04%) 2.69 fm $r_T = 2.73 \text{ fm}$ 8.1 MeV 0	18O 2×10^4 (0.2%) 2.77 fm $r_T = 2.74 \text{ fm}$ 8.1 MeV 0
PERIOD TWO	19F 4×10^2 (100%) 2.90 fm $r_T = 2.63 \text{ fm}$ 10.5 MeV +2.63	20Ne* 1.2×10^6 (90.5%) 3.01 fm $r_T = 2.84 \text{ fm}$ 12.8 MeV 0	21Ne 3.9×10^3 (0.3%) 2.97 fm $r_T = 2.91 \text{ fm}$ 6.8 MeV -0.662	22Ne 1.2×10^5 (9.2%) 2.95 fm $r_T = 2.92 \text{ fm}$ 10.3 MeV 0	23Na 2×10^4 (100%) 2.99 fm $r_T = 2.83 \text{ fm}$ 8.8 MeV +2.22	24Mg* 4.8×10^5 (79.0%) 3.06 fm $r_T = 2.82 \text{ fm}$ 11.7 MeV 0	25Mg 6×10^4 (10.0%) 3.03 fm $r_T = 2.85 \text{ fm}$ 7.3 MeV -0.855	26Mg 6×10^4 (11.0%) 3.03 fm $r_T = 2.82 \text{ fm}$ 11.1 MeV 0	27Al 5×10^4 (100%) 3.06 fm $r_T = 3.11 \text{ fm}$ 8.3 MeV +3.64	28Si* 6.3×10^5 (92.2%) 3.12 fm $r_T = 3.13 \text{ fm}$ 11.7 MeV 0	29Si 3.5×10^4 (4.7%) 3.12 fm $r_T = 3.12 \text{ fm}$ 8.5 MeV -0.555	30Si 2.1×10^4 (3.1%) 3.13 fm $r_T = 3.13 \text{ fm}$ 10.6 MeV 0
PERIOD THREE	31P 7×10^3 (100%) 3.19 fm $r_T = 3.13 \text{ fm}$ 12.4 MeV +1.13	32S* 4.8×10^5 (94.9%) 3.26 fm $r_T = 3.30 \text{ fm}$ 8.9 MeV 0	33S 4×10^3 (0.8%) unknown $r_T = 3.30 \text{ fm}$ 8.7 MeV +0.64	34S 2.2×10^4 (4.3%) 3.28 fm $r_T = 3.30 \text{ fm}$ 11.4 MeV 0	35Cl 7.6×10^2 (75.8%) 3.37 fm $r_T = 3.41 \text{ fm}$ 6.3 MeV +0.822	36Ar* 6×10^2 (0.3%) 3.39 fm $r_T = 3.41 \text{ fm}$ 8.5 MeV 0	Lightest Nuclides (qualitative quark view)					
						2H* 1.2×10^5 (0.01%) 2.13 fm $r_T = 2.11 \text{ fm}$ 2.22 MeV +0.857	3He 4.6×10^4 (0.0002%) 1.97 fm $r_T = 1.92 \text{ fm}$ 6.23 MeV -2.13	4He* 2.3×10^8 (99.9%) 1.68 fm $r_T = 1.63 \text{ fm}$ 20.58 MeV 0	6Li* 4.6×10^1 (7.6%) 2.59 fm $r_T = 2.42 \text{ fm}$ 3.7 MeV +0.822	1H 7.5×10^0 0.84 fm chiral plane of symmetry IAEA radius model radius separation energy magnetic moment		

either end-over-end tumbling (r_T) or precessing (r_P), as discussed above. Below the charge radius prediction is the nucleon separation energy, which is determined from the difference in total binding energy between the nuclide of interest and the previous stable nuclide (1 amu lighter).

The bottom number in each nuclides box is the nuclear magnetic moment (μ), an experimentally determined value. [37] It is thought to derive from the spin of nucleons and their quarks but is not simply the sum of quark magnetic moments. [38] While spin is an intrinsic form of angular momentum, the nuclear magnetic moment also depends on orbital angular momentum, which relates to how a nucleus rotates in space. [39] This is particularly relevant when considering that the best-fit manner of rotation of most nuclides in Table 1 is a tumbling rotation; for others, it is precessing, and for some it can be either. The μ equals zero due to nucleon pairing effects when the numbers of protons and neutrons are both even. Since stable nuclides through ^{36}Ar increase one nucleon at a time, every other magnetic moment will equal zero, beginning with ^{16}O . Otherwise, the nuclear magnetic moment μ is unique for each nuclide and varies in sign and magnitude as mass number increases.

The key to Table 1 is shown in the table's lower right corner. Neutrons are white, and protons are red. The table begins with ^7Li , corresponding to the linear portion of the radius-to-mass plot depicted in figure 1. Beginning with ^7L , structures evolve by the incremental and predictable addition of nucleons and demonstrate a structural periodicity that recurs every 12 nuclides, as shown. This is in contrast to the irregular shapes of the lightest nuclides depicted in the lower right of the table. Structural periodicity corresponds to columnar trends in nucleon binding energies and nuclear magnetic moments, to be discussed in greater detail below.

The Roman numerals across the top of Table 1 refer to the “anisotrope” group number, defined in this context as the number of nucleons common to the anisotropic end of each nuclide in a column. The anisotrope is depicted in red and white nucleons, while the other end of the nuclear cylinder remains essentially inert and is depicted in gray and pink nucleons below the anisotrope. With the exception of the boron nuclides, the anisotrope group number additionally corresponds to the unique nucleon configurations present on the evolving end of the anisotropic cylinder. As described in the Model section, the anisotrope guides the sequence and occupancy of nucleons, and best-fit radii result when nucleons are added only to the anisotrope end of the evolving nuclear cylinder. As there are twelve

anisotope groups (Roman numerals), the anisotope configurations include up to 12 nucleons arranged within up to two stacked 6-nucleon rings.

There are three Periods listed down the left side of Table 1. The structure of the anisotope generally evolves in the same way across each Period by adding one nucleon at a time in a predictable configuration. The boron isotopes ^{10}B and ^{11}B represent an exception; however, their smaller-than-expected experimental radii present a challenge to structural elucidation, which was resolved by placing a ^4He ring nucleus within the center of each, as shown. This structural contortion and potential weakness in the structure may account for boron's low cosmic abundance (discussed previously). [40] As an aside, the inclusion of neutrons and alpha particles within the center of the nuclide may set a precedent for the increased density of nuclide structures above ^{36}Ar .

The eight equinucleonic ($Z=N$) nuclides through ^{36}Ar exhibit a chiral bilateral plane of symmetry (double blue line) and comprise 99.5% of polynucleonic baryonic matter. Above ^{35}Cl , however, structural symmetry is no longer a sensitive and specific predictor of abundance. Within the model, ^{36}Ar is point-symmetrical but comprises only 0.3% of elemental Ar, while ^{40}Ar is argon's most abundant isotope at 99.66%. The equal numbers of protons and neutrons in ^6Li do not result in a rigid, symmetrical nucleus through which a plane of symmetry may be drawn. ^{10}B is also asymmetrical in spite of its equal protons/neutron numbers (as shown), precluding a plane of symmetry. Nuclei containing a neutron inclusion, such as ^{13}C , are symmetrical but do not contain a chiral plane of symmetry in which protons reflect neutrons on opposite sides of a chiral plane of symmetry.

4. Discussion

The alternating nucleon structures featured in Table 1 were assembled using first principles and empirically accepted nucleon size, shape, and distance of separation, guided by the known stability of the proton-neutron NN interaction. The final step in structural elucidation was the vetting of a structure's calculated predicted radius against the experimental charge radius, and the structures correlating best with IAEA-accepted charge radii were included in Table 1. Compliance with accepted charge radii generated a mix of symmetrical and asymmetrical structures, and bilateral structural symmetry emerges as a sensitive and specific predictor of light nuclide abundance.

4.1. The 12-nuclide periodicity.

The sequence of stable light nuclides progresses one amu (nucleon) at a time, skipping the five and eight-amu nuclides. The process of structural elucidation proceeded the same way. According to the method described above, each provisional nuclide was vetted against the experimental charge radius, and the one correlating most closely with the experimental appears in Table 1. During the process of elucidation, certain structural patterns emerged, recurring with predictable periodicity. Starting from an open ring, the next nucleon would occupy the center, the second added nucleon would pull the center nucleon onto a parallel ring, and the sequence would add nucleons incrementally to become three, four, and five nucleon sequences before finally adding a sixth nucleon to complete a parallel six-nucleon ring identical to ^6Li . The process would then repeat itself.

Within the nuclides ^7Li , ^{13}C , ^{19}F , ^{25}Mg , and ^{31}P , each successive nuclide is 6 amu greater than the last. The anisotope of each structure is the same, each having a single neutron within a nucleus comprising one or more complete rings, and the five nuclides display structural periodicity. If nuclear physical properties spring from nuclear structure the way that the atomic physical properties (like ionization energy or ionic radius) derive from electron orbital structure, then nuclear properties (such as μ and nucleon separation energy) should exhibit respective periodicity. The μ 's of these five nuclides are (respectively) +3.26, +0.702, +2.63, -0.855, and +1.13, while the respective nucleon separation energies (in MeV) are 7.2, 5.0, 10.5, 7.3, and 12.4. Neither sequence reflects clear trends in μ or nucleon separation energy, however. Neither do the other six nucleon sequences beginning with ^8Be , ^9Be , ^{10}B , ^{11}B , and ^{12}C exhibit convincing trends in nucleon separation energy, or non-zero trends in μ .

This is in contrast to the evidence for columnar trends in μ and nucleon separation energy in Table 1, organized around 12-nucleon periodicity. Group I, for example, demonstrates an increasing trend in nucleon separation energy and a decreasing trend in μ . The columnar trends in the nuclear magnetic moment tend to decrease in magnitude down an anisotope group while maintaining the sign or staying

at zero, with the exception of groups VII and IX, in which the sign differs between periods. The sign disparity in groups VII and IX between Periods I and II may relate to the effects of precessing rotation on the magnetic moments of the Period One nuclides.

These trends are not like the two-dimensional trends found in the Periodic Table of the Elements (such as ionization energy or atomic radius), which trend in both the horizontal and vertical directions. As Table 1 demonstrates, nuclear trends in nucleon separation energy are one-dimensional and confined to a column. The trends vary from group to group but exhibit a conspicuous pattern. The trend is downward in group I, and upward in group II. Thereafter, the trends alternate regularly by two so that the trend in groups III and IV is **up**, groups V and VI **down**, groups VII and VIII **up**, groups IX and X **down**, and finally, groups XI and XII **up**. The cause of this pattern warrants further investigation.

4.2. *en bloc* movement of nucleon substrates

The correlation between the accepted nuclear radius and the prediction is statistically near-perfect but falls short for the nuclides ${}^6\text{Li}$, ${}^{19}\text{F}$, ${}^{20}\text{Ne}$, ${}^{23}\text{Na}$, and the three stable isotopes of magnesium. In figure 6, these nuclides represent gaps between the model prediction (red dashed line) and the experimental charge radius (solid black line), and model predictions underestimate the experimental radius. The underestimation may result from the *en bloc* movement of nucleon substructures. The proposed structure of ${}^{19}\text{F}$ may contain two distinct substructures: a ${}^7\text{Li}$ bound to a ${}^{12}\text{C}$. The low abundance of ${}^{19}\text{F}$ may suggest that the association is relatively fragile if each substructure possesses the capacity to move independently relative to the other. The ${}^7\text{Li}$ may sublux or slide over the top of the ${}^{12}\text{C}$, resulting in an elongation of the experimental radius. The structure of ${}^{24}\text{Mg}$ may comprise a bound state of two ${}^{12}\text{C}$ nuclei, the nucleons of each moving *en bloc* relative to the other. One ${}^{12}\text{C}$ might sublux over the other during nuclear rotation, resulting in elongation and a larger-than-predicted experimental charge radius. A ≈ 0.3 fm lateral shift of one ${}^{12}\text{C}$ relative to the other would be sufficient to bring the predicted radius of ${}^{24}\text{Mg}$ (2.82 fm) in line with the experimental (3.06 fm).

4.3. Steric selection anomalies

There are seven (out of 33) instances where the model predicts that the addition of a proton will result in the next stable nuclide, but instead, the addition of a neutron results in the next stable nuclide. The deuteron adds a proton to produce stable ${}^3\text{He}$, for example, whereas the model anticipates the addition of a neutron to form a triton (which is unstable). In another example, the model's steric selection mechanism anticipates the addition of a proton to ${}^7\text{Li}$ to produce ${}^8\text{Be}$, but ${}^8\text{Be}$ is unstable. Likewise, the model anticipates the addition of a proton to ${}^{17}\text{O}$, ${}^{21}\text{Ne}$, ${}^{25}\text{Mg}$, ${}^{29}\text{Si}$, and ${}^{33}\text{S}$, but in each of these five instances, the stable isotope arises instead from the addition of a neutron resulting in ${}^{18}\text{O}$, ${}^{22}\text{Ne}$, ${}^{26}\text{Mg}$, ${}^{30}\text{Si}$, and ${}^{34}\text{S}$. In total, the model's steric selection mechanism predicts the next stable nuclide in 26 of the 33 instances. Importantly, the nuclides resulting from these 26 successful predictions constitute 99.39% of the ordinary polynucleonic matter of the universe by mass, while the seven nuclides resulting from the unanticipated addition of a neutron constitute a scant 0.09% of the polynucleonic mass of the universe.

5. Conclusion

The vast majority of ordinary baryonic matter aside from hydrogen comprises just eight nuclides: ${}^4\text{He}$, ${}^{12}\text{C}$, ${}^{14}\text{N}$, ${}^{16}\text{O}$, ${}^{20}\text{Ne}$, ${}^{24}\text{Mg}$, ${}^{28}\text{Si}$, and ${}^{32}\text{S}$. They all contain equal numbers of protons and neutrons. The relevance of these "Big Eight" nuclides to a complete understanding of nuclear science cannot be overstated.

Symmetry is ubiquitous in nature, and evidence abounds that structural symmetry confers structural stability. [41] [42] [43] [44] Within the model, bilateral structural symmetry develops as a sensitive and specific predictor of nuclide abundance, and structural *asymmetry* emerges as a predictor of cosmic scarcity. The conclusion of this paper is that matter aggregates in alternating nucleon sequences to optimize the formation of stable NN interactions and maximize the number of pn SRC pairs. Nuclides having equal numbers of protons and neutrons intrinsically contain the maximum number of pn SRC pairs. The alternation of nucleons implicitly generates the observed equal numbers of protons and neutrons within the most abundant forms of matter. Within the model, the equality of

proton/neutron numbers manifests as structural symmetry, conferring to the eight superabundant equinucleonic nuclides sufficient kinetic stability to withstand highly exothermic Big Bang or stellar nuclear reaction conditions and emerge in high relative cosmic abundance.

Acknowledgments

Special thanks to Timothy L. Lohof, Ph.D. candidate at Geneva Graduate Institute, for assistance in researching the literature review. Also, thanks to Daniel J. Glenn, principal architect at 7 Directions Architecture, for literature recommendations regarding structural symmetry.

References

- [1] P. Tipler and R. Llewellyn, "11-2 Ground-State Properties of Nuclei," in *Modern Physics, 6th Edition*, New York, W. H. Freeman and Company, 2012, p. 497.
- [2] C. Alexandrou, C. N. Papanicolas and M. Vanderhaegen, "The Shape of Hadrons," *Rev. Mod. Phys.*, vol. 84, p. 1231, 2012.
- [3] J. M. B. Kellogg , . I. I. Rabi, N. F. Ramsey and J. R. Zacharias, "An Electrical Quadrupole Moment of the Deuteron," *Physical Review*, 1 February 1939.
- [4] J. S. McCarthy, I. Sick and R. R. Whitney, "Electromagnetic structure of the helium isotopes," *Phys. Rev. C*, vol. 15, no. 4, pp. 1396-1414, 1977.
- [5] A. Lovato, S. Gandolfi, R. Butler, J. Carlson and et all, "Charge Form Factor and Sum Rules of Electromagnetic Response Functions in ^{12}C ," *Phys. Rev. Lett.* 111, 092501, 2013.
- [6] R. Hofstadter, "Hofstadter Nobel Lecture, Figure 8," 11 Dec. 1961. [Online]. Available: <https://www.nobelprize.org/prizes/physics/1961/hofstadter/lecture/>. [Accessed 16 Feb. 2023].
- [7] I. Angelis and K. P. Marinova, "2013 Table of Experimental Ground State Charge Radii," *At. Data Nucl.*, pp. Data Tables 99, 69, 2013.
- [8] G. A. M. E. P. a. L. B. W. O. Hen, *Rev. Mod. Phys.*, Vols. 89, 045002, 2017.
- [9] R. B. W. S. C. P. a. J. C. R. Schiavilla, *Phys. Rev. Lett.*, vol. 98, no. 132501, 2007.
- [10] I. Korover, A. W. Denniston and A. e. a. Kiral, "Observation of large missing-momentum (e^- , e^+ , p) cross-section scaling and the onset of correlated-pair dominance in nuclei," *Physical Review C* 107(C), June 2023.
- [11] K. J. R. ROSMAN and P. D. P. TAYLOR, "ISOTOPIC COMPOSITIONS OF THE ELEMENTS 1997," IUPAC, Great Britain, 1977.
- [12] M. G. Mayer, "Maria Goeppert Mayer Nobel Lecture," 1963. [Online]. Available: <https://www.nobelprize.org/prizes/physics/1963/mayer/lecture/>. [Accessed 10 July 2024].
- [13] M. G. Mayer and J. H. Jensen, Elementary Theory of Nuclear Shell Structure, New York: Wiley, 1955.
- [14] G. Royer and P. Eudes, "Alpha clustering and nuclear molecules in ^{8}Be , ^{12}C , ^{16}O ^{20}Ne , and ^{32}S ," *Journal of Physics: Conference Series*, vol. 863, p. 012012, 2017.
- [15] P. M. Chaikin and T. C. Lubensky, rinciples of condensed matter physics (4th print ed.). ISBN 978-0-521-79450-3., Cambridge: Cambridge University Press, 2007.
- [16] L. Carlson and et al, "Quantum Monte Carlo methods for modern physics," *Reviews of modern physics*, vol. 87, no. 3, pp. 1067-1118, 2015.
- [17] M. P. Fewell, "The atomic nuclide with the highest mean binding energy," *Am. J. Phys.*, vol. 63, no. 7, p. 653–658, 1995.
- [18] M. Salvadori, "Dynamic Loads," in *Why Buildings Stand Up*, London, WW Norton, 1980, p. 45.
- [19] A. H. R. D. H. a. S. E. W. T. Rauscher, "NUCLEOSYNTHESIS IN MASSIVE STARS WITH IMPROVED NUCLEAR AND STELLAR PHYSICS," p. 576:323–348, 2002 September 1.

- [20] J. A. H. R. M. Meneguzzi, "The production of the elements Li, Be, B by galactic cosmic rays in space and its relation with stellar observations," *Astronomy and Astrophysics*, vol. 15, pp. 337-359, 1971.
- [21] I. Angeli, "1999 TABLE OF NUCLEAR ROOT MEAN SQUARE CHARGE RADII*," International Atomic Energy Agency, Hungary, 1999.
- [22] R. B. Wiringa, V. G. J. Stoks and R. Schiavilla, "Accurate nucleon-nucleon potential with charge-independence breaking," *Phys. Rev. C: Nucl. Phys.*, vol. 51, no. 38, 1995.
- [23] B. S. Ishkhanova, M. E. Stepanova and T. Y. Tretyakova, "Nucleon Pairing in Atomic Nuclei," *Moscow University Physics Bulletin*, vol. 69, no. 1, pp. 1-20, 2014.
- [24] A. M. Bernstein, "Deviation of the Nucleon Shape From Spherical Symmetry: Experimental Status," *Eur.Phys.J.*, vol. A17, pp. 349-355, 2003.
- [25] L. Tiator, D. Drechsel, S. Kamalov and S. Yang, "Electromagnetic form factors of the $\Delta(1232)$ excitation," *Eur. Phys. J. A*, Vols. 17: 357-363, 2003.
- [26] E. M. H. A. J. Buchmann, "Intrinsic quadrupole moment of the nucleon," *Phys.Rev.C*, vol. 63, no. DOI: 10.1103/PhysRevC.63.015202, 2001.
- [27] A. Buchmann, "Nucleon deformation and atomic spectroscopy," *Can.J.Phys*, vol. 83, no. 4, pp. 455-465, 2005.
- [28] A. J. Buchmann and E. M. Henley, "Intrinsic quadrupole moment of the nucleon," *Phys. Rev. C*, vol. 63, p. 015202, 2000.
- [29] NIST, "proton rms charge radius," NIST, 2022. [Online]. [Accessed 14 July 2024].
- [30] A. Coc, P. Descouvemont, K. A. Olive, J.-P. Uzan and E. Vangioni, "Variation of fundamental constants and the role of $A = 5$ and $A = 8$ nuclei on primordial nucleosynthesis," *Phys. Rev. D* 86, 043529, 24 August 2012.
- [31] P. Riggs, "Revisiting Standing Waves on a Circular Path," *The Physics Teacher*, vol. 59, pp. 100-102, 2021.
- [32] W. Nörtershäuser, D. Tiedemann, M. Žáková and et al, "Nuclear Charge Radii of Be7,9,10 and the One-Neutron Halo Nucleus Be11," *Physical Review Letters*, vol. 102, no. 6, 2009.
- [33] M. Salvadori, "Bridges," in *Why buildings stand up*, London, WW Norton, 1980, pp. 144-164.
- [34] V. B. HAMMER and P. PEDERSEN, "OPTIMIZATION OF LAMINATE STRENGTH," in *In: Bestle, D., Schiehlen, W. (eds) IUTAM Symposium on Optimization of Mechanical Systems. Solid Mechanics and its Applications*, vol 43. Springer, Dordrecht. , 1996.
- [35] I. Angeli and K. P. Marinova, "Table of Experimental Ground State Charge Radii," *At. Data Nucl.*, pp. Data Tables 99, 69, 2013.
- [36] R. Feynman, "The Feynman Lectures on Physics - Chapter 20 Rotations in Space," California Institute of Technology, 1963. [Online]. Available: https://www.feynmanlectures.caltech.edu/I_20.html. [Accessed 2 January 2022].
- [37] K. S. Krane, "Extensions and applications," in *Introductory Nuclear Physics*, New York, Wiley, 1988, p. 625.
- [38] E. Cartlidge, "The spin of a proton," *Phys. World*, vol. 28, no. 6, pp. 28-32, 2015.
- [39] L. LANDAU and E. LIFSHITZ, "CHAPTER VIII - SPIN," in *Quantum Mechanics*, Elsevier, 1977, pp. 197-224.
- [40] John Emsley, *Nature's Building Blocks: An A-Z Guide to the Elements*, Oxford: Oxford University Press, 2001.
- [41] T. Blundell and N. Srinivasan, "Symmetry, stability, and dynamics of multidomain and multicomponent protein systems," *PNAS*, vol. 93, no. 25, pp. 14243-14248, 1996.

- [42] Y. Chen, P. Sareh and J. Feng, "Effective insights into the geometric stability of symmetric skeletal structures under symmetric variations," *International Journal of Solids and Structures*, vol. 69–70, pp. 277-290, September 2015.
- [43] M. Salvadori, *Why Buildings Stand Up: The Strength of Architecture*, New York: W. W. Norton and Company, Inc., 1990.
- [44] P. Rajput, K. Dabheka, P. Pawade, I. Khedikar and N. Pawar, "Review on “Seismic performance analysis of symmetric and asymmetric structure with and without base isolation under bidirectional ground motion and subjected to torsion”," in *ADVANCES IN SUSTAINABLE CONSTRUCTION MATERIALS*, Guntur, India, 2022.
- [45] Tipler, "11-2 Ground-State Properties of Nuclei," in *Modern Physics*, p. 497.
- [46] G. Gamow, "Mass Defect Curve and Nuclear Constitution," *Proceedings of the Royal Society of London*, vol. 126, no. 803, pp. 632-644, 1930.
- [47] M. Meneguzzi, J. Audouze and H. Reeves, "The production of the elements Li, Be, B by galactic cosmic rays in space and its relation with stellar observations," *Astronomy and Astrophysics*, vol. 15, no. 337, 1971.
- [48] P. Strathern, in *Mendeleev's Dream*, New York, Pegasus Books Ltd., 2001, p. 133.
- [49] A. Bohr and B. Mottelson, *Nuclear Structure II*, Reading: A. Benjamin, 1975.
- [50] N. Cook, *Models of the Atomic Nucleus*, London: Springer, 2006.
- [51] L. Tiator, D. Drechsel, S. Kamalov and S. Yang, "Electromagnetic form factors of the $\Delta(1232)$ excitation," *Eur. Phys. J. A*, vol. 17, pp. 357-363, 2003.
- [52] G. Blanpied et al, "N Δ transition and proton polarizabilities from measurements of $p(\rightarrow \gamma, \gamma)$, $p(\rightarrow \gamma, \pi^0)$, and $p(\rightarrow \gamma, \pi^+)$," *Phys. Rev. C* 64, vol. 64, no. 2, 2001.
- [53] NIST, "deuteron rms charge radius," 2022. [Online]. [Accessed 14 July 2024].
- [54] G. Audi, F. G. Kondev, M. Wang, W. J. Huang and S. Naimi, "The NUBASE2016 evaluation of nuclear properties," *Chinese Physics C*. 41 (3): 030001., 2017.
- [55] Y. Chu, Z. Ren, Z. Wang and T. Dong, "Central depression of nuclear charge density distribution," *Phys. Rev. C.*, vol. 82, p. 024320, 2010.
- [56] APPENDIX D: AQM vs GFMC RADIUS PREDICTIONS.
- [57] APPENDIX A: COMPARISON OF AQM AND GFMC ASSUMPTIONS.
- [58] Bob Kahn, Editor, GP-B Science Team, "Gravity Probe-B Mission News - Polhode Motion in the GP-B Gyros," Stanford Information Technology Services, November 2006. [Online]. Available: https://einstein.stanford.edu/highlights/hl_polhode_story.html. [Accessed 2 January 2022].
- [59] D. J. Griffiths, " Particles (Nuclear physics)," in *Introduction to elementary particles*, Wiley & Sons, 2008, p. 135.
- [60] APPENDIX D: AQM RADIUS PREDICTIONS.
- [61] APPENDIX C: COMPARISON OF PERIODIC SEQUENCES LENGTHS FOR MAGNETIC MOMENT AND NUCLEOSYNTHESIS PERIODICITIES.
- [62] High Energy Physics Division, "High Energy Physics Division," dbserv.pnpi.spb.ru, [Online]. Available: <http://dbserv.pnpi.spb.ru/elbib/tblisot/toi98/www/astro/table2.pdf>. [Accessed 1 July 2023].
- [63] Bohr, A. and Mottelson, B., *Nuclear Structure*, Reading, MA: Benjamin, 1969.